Journal for ImmunoTherapy of Cancer

Efficient targeting of NY-ESO-1 tumor antigen to human cDC1s by lymphotactin results in cross-presentation and antigen-specific T cell expansion

Camille Le Gall ,[1,2] Anna Cammarata ,[1] Lukas de Haas ,[1] Iván Ramos-Tomillero ,[1,3] Jorge Cuenca-Escalona ,[1] Kayleigh Schouren ,[1] Zacharias Wijfjes ,[1,3] Anouk M D Becker ,[1] Johanna Bödder ,[1] Yusuf Dölen ,[1,2] I Jolanda M de Vries ,[1] Carl G Figdor ,[1,2] Georgina Flórez-Grau ,[1] Martijn Verdoes [1,3]

To cite: Le Gall C, Cammarata A, de Haas L, *et al*. Efficient targeting of NY-ESO-1 tumor antigen to human cDC1s by lymphotactin results in cross-presentation and antigen-specific T cell expansion. *Journal for ImmunoTherapy of Cancer* 2022;**10**:e004309. doi:10.1136/jitc-2021-004309

► Additional supplemental material is published online only. To view, please visit the journal online (http://dx.doi.org/10.1136/jitc-2021-004309).

GF-G and MV are joint senior authors.

Accepted 15 March 2022

For numbered affiliations see end of article.

Correspondence to
Dr Martijn Verdoes; Martijn.Verdoes@radboudumc.nl

Dr Georgina Flórez-Grau; Georgina.Florez-Grau@radboudumc.nl

ABSTRACT

Background Type 1 conventional dendritic cells (cDC1s) are characterized by their ability to induce potent $CD8^+$ T cell responses. In efforts to generate novel vaccination strategies, notably against cancer, human cDC1s emerge as an ideal target to deliver antigens. cDC1s uniquely express XCR1, a seven transmembrane G protein-coupled receptor. Due to its restricted expression and endocytic nature, XCR1 represents an attractive receptor to mediate antigen-delivery to human cDC1s.

Methods To explore tumor antigen delivery to human cDC1s, we used an engineered version of XCR1-binding lymphotactin (XCL1), XCL1(CC3). Site-specific sortase-mediated transpeptidation was performed to conjugate XCL1(CC3) to an analog of the HLA-A*02:01 epitope of the cancer testis antigen New York Esophageal Squamous Cell Carcinoma-1 (NY-ESO-1). While poor epitope solubility prevented isolation of stable XCL1-antigen conjugates, incorporation of a single polyethylene glycol (PEG) chain upstream of the epitope-containing peptide enabled generation of soluble XCL1(CC3)-antigen fusion constructs. Binding and chemotactic characteristics of the XCL1-antigen conjugate, as well as its ability to induce antigen-specific $CD8^+$ T cell activation by cDC1s, was assessed.

Results PEGylated XCL1(CC3)-antigen conjugates retained binding to XCR1, and induced cDC1 chemoattraction in vitro. The model epitope was efficiently cross-presented by human cDC1s to activate NY-ESO-1-specific $CD8^+$ T cells. Importantly, vaccine activity was increased by targeting XCR1 at the surface of cDC1s.

Conclusion Our results present a novel strategy for the generation of targeted vaccines fused to insoluble antigens. Moreover, our data emphasize the potential of targeting XCR1 at the surface of primary human cDC1s to induce potent $CD8^+$ T cell responses.

Key messages

What is already known on this topic

► XCR1 expressing type 1 conventional dendritic cells (cDC1s) are known for their increased ability to prime $CD8^+$ T cells compared with other DC subsets, and thus considered a promising target for cancer vaccines to induce tumor antigen-specific cytotoxic T cell responses. While this is well-established in mouse, studies on human cDC1s are scarce.

What this study adds

► Our results demonstrate the potential of lymphotactin as an XCR1-targeting agent that can be easily conjugated to antigens and induce potent $CD8^+$ T cell responses. In addition, we developed a practical solution allowing the synthesis of otherwise insoluble cDC1-targeted vaccines.

How this study might affect research, practice, or policy

► The findings presented here will facilitate the generation of targeted protein-based (cancer) vaccines with notoriously poorly soluble epitopes and encourage further investigation of XCR1 as a target on human cDC1s.

INTRODUCTION

Conventional dendritic cell (DCs) type 1 (cDC1s) are the rarest subset of DCs, making up only 0.03% of human peripheral blood mononuclear cells (PBMCs). cDC1s are characterized by their expression of CD141 (BDCA-3), CLEC9A (DNGR-1) and X-C motif chemokine receptor 1 (XCR1),[1 2] and additionally express high levels of Toll-like receptor (TLR) 3 and TLR7. The scarcity of these cells in peripheral blood renders the study of human cDC1s cumbersome, thus most functional studies have been performed on their murine cDC1s counterpart. *Batf3*-deficient mice selectively lacking cDC1s are

unable to mount an effective cytotoxic immune response against viruses and tumors.[3] cDC1s have been shown in vitro and in vivo to excel at cross-presentation of extracellular[4] and dead-cell associated[5] antigens to $CD8^+$ T cells. Human $CD141^+CLEC9A^+XCR1^+$ have been shown to similarly excel at cross-presentation.[6 7] This cross-presenting capacity makes human cDC1s an optimal cell population for eliciting cytotoxic immune responses against tumors.

cDC1s uniquely express XCR1, a chemokine receptor allowing cells to specifically migrate toward lymphotactin, commonly referred to as X-C motif chemokine ligand 1 (XCL1). XCL1 is a 12 kDa chemokine mainly secreted by activated cytotoxic $CD8^+$ T and NK cells. The XCR1/XCL1 axis is a major regulator of cytotoxic immune responses. Mice lacking either XCR1 or XCL1 have deficient cytotoxic T cell responses,[8] but interestingly also lack the ability to generate regulatory T cells.[9] XCL1 is thus able to modulate the spatial location and function of both T cells and DCs. Binding of XCL1 to the orthosteric site of XCR1 triggers Ca^{2+} efflux from the endoplasmic reticulum (ER), leading to cytoskeleton remodeling and cell migration,[10] followed by XCR1 desensitization and internalization to early endosomes.[11] It is hypothesized that by following a XCL1 chemotactic gradient, $XCR1^+$ cDC1s can migrate toward the site of inflammation, where they take up antigens. Downregulation of XCR1, and activation-induced expression of CCR7, enables subsequent migration to the lymph node,[12] where cDC1s are able to prime T cells. Due to the restricted expression of XCR1 on cDC1s, and its endocytic nature, XCR1 represents a highly attractive target for the delivery of tumor antigens in vivo, and to induce $CD8^+$ T cell responses.[13–15] We chose to use its ligand, XCL1, as a tumor antigen delivery moiety.[14 16 17]

XCL1 is the only member of its family in mouse. In humans, XCL2 (NC_000001.11 (168540768.168543997, complement)) is a paralog chemokine present in the same locus as XCL1 (NC_000001.11 (168574128.168582069)). XCL1 and XCL2 have the particularity to present only one disulfide bond. This particularity allows them to adopt two conformations under normal physiological conditions: a monomeric α-β XCR1-binding fold, and an all-β dimeric glycosaminoglycan (GAG)-binding fold.[18 19] Point mutations of two valine residues into cysteine residues (V21C/V59C) locks XCL1 into its XCR1 agonist α-β fold.[19 20] We generated an engineered XCR1 ligand, based on the V21C/V59C fold (XCL1(CC3)), further modified by fusing it C-terminally to a LPETGG sortag motif, allowing for site-specific chemoenzymatic modification to virtually any payload.[21]

To build and evaluate the activity of a cDC1-targeting vaccine, we set out to conjugate XCL1(CC3) to an epitope of the well-characterized tumor antigen New York Esophageal Squamous Cell Carcinoma-1 (NY-ESO-1). This cancer testis tumor-associated antigen (TAA) is aberrantly expressed by a large proportion of patients in several malignancies, including multiple myeloma (60%),[22] neuroblastoma (82%),[23] and melanoma (45%).[24] NY-ESO-1-derived peptide (157-165) (^{157}SLLMWITQ^{165}C, in short S7C) has been identified as an immunodominant epitope giving rise to antigen-specific $CD8^+$ T cell responses in HLA-A*02:01 patients.[25] S7C is notoriously highly hydrophobic (hydrophobicity=35.77, GRAVY=1.18), and dimer formation by P9 cysteine-pairing causes problems in preparation and formulation of S7C-based vaccines.[26] Despite their unfavorable biochemical characteristics, NY-ESO-1-derived epitopes are highly promising for off-the-shelf cancer vaccines, due to NY-ESO-1 high prevalence. To avoid cysteine pairing, we chose to use an analog of S7C as model antigen (^{157}SLLMWITQ(^{165}Abu) (S7Abu), Abu=L-2-aminobutyric acid), which was shown to bind HLA-A*02:01, and to be recognized by S7C-specific patient-derived $CD8^+$ T cells.[26] We aimed at functionalizing XCL1 with the S7Abu epitope and evaluating the potential of such a targeting approach to activate antigen-specific $CD8^+$ T cells via human $XCR1^+$ cDC1s.

MATERIALS AND METHODS

XCL1(CC3) design and cloning

pET28a(+) backbone with NdeI and EcoRI cloning sites was obtained by PCR of an existing template (Sec22b in pET28a(+), provided by Dr. Martin ter Beest) using 5'–CCGAGTCACTCATATGGCTGCCGCGCGGCACC–3' and 5'– ATACATACGAGAATTCGCGGCCGCACTC GAGCACCA –3'. 6×His-SUMO-XCL1(CC3)-FLAG was ordered as a gBlock from IDT DNA Technologies and cloned in digested pET28a(+) at NdeI (R0111, New England Biolabs) and EcoRI (R0101, New England Biolabs) sites.

Chemicals

Chemicals used to produce XCL1, sdAb and sortase, in peptide synthesis, for HPLC purification and analysis, and for cell isolation were obtained from Merck/Sigma Aldrich, unless stated otherwise.

XCL1 production and purification

XCL1(CC3) was produced in BL21(DE3) *Escherichia coli* by adapting a published protocol.[20] Bacteria were thawed on ice and incubated for 5 min with 100 ng of XCL1 in pET28a(+) plasmid. Transformation was performed by heat shock in a water bath (42°C, 42 s), followed by 3 min incubation on ice. 1 mL LB was added, and bacteria were left to recover (1 hour, 37°C, 220 rpm). Bacteria were transferred to 50 mL of selective media (2×TY + 50 $\mu g \cdot mL^{-1}$ kanamycin) and grown overnight (16 hours, 30°C, 220 rpm). The next day, the suspension was inoculated in selective media to OD_{600}~0.05, and bacteria were grown (37°C, 220 rpm), until reaching OD_{600}~0.6. XCL1 production was induced by addition of Isopropyl β-D-1-thiogalactopyranoside (IPTG) to a concentration of 1 mM, and subsequent culturing (5 hours, 30°C, 220 rpm). Bacteria were collected by centrifugation (20 min, 4°C, 3 000 g), supernatant was discarded, and pellets were frozen at −20°C until further isolation. Pellets were thawed at room temperature (RT) and resuspended

in lysis buffer (50 mM sodium phosphate pH=8.0, 300 mM NaCl, 10 mM imidazole, 20 mM DTT, 20 µg·mL^{-1} protease inhibitor cocktail (4693159001, Roche), 200 U·mL^{-1} DNAseI (P5224, Abnova)) (20 mL per 1 L original culture). Suspension was sonicated on ice (3×30 s, 25% amplitude), and spun down (30 min, 4°C, 8 600 g). Supernatant (soluble fraction) was collected, and pellet was resuspended in resuspension/wash buffer (50 mM sodium phosphate pH=8.0, 6 M guanidine hydrochloride, 300 mM NaCl, 10 mM imidazole, 20 mM DTT) (20 mL per 1 L of original culture) to lyse inclusion bodies (1 hour, 37°C) on an end-over-end shaker. Suspension was spun down (30 min, RT, 8 600 g), and supernatant (insoluble fraction) was collected, and pooled with the soluble fraction. Lysate was incubated with 2 mL of pre-washed Ni-NTA resin (30230, Quiagen) (1 hour, RT) on an end-over-end shaker. Suspension was diluted 1:1 (v/v) with resuspension/wash buffer and transferred to disposable columns (7321010, Bio-Rad). Resin was washed with 25 CV resuspension/wash buffer and eluted with 4 CV elution buffer (100 mM sodium acetate pH=4.5, 6 M guanidine HCl, 300 mM NaCl, 10 mM imidazole). Elution was refolded by infinite dilution in refolding buffer (20 mM Tris pH=8.0, 200 mM NaCl, 10 mM cysteine, 0.5 mM cystine) overnight at RT. Refolded mixture was concentrated on a 10 kDa Amicon spin filter (cycles of 10 min, RT, 3 000 g) until reaching less than 2 mL of volume. SUMO-XCL1 was then diluted with (20 mM Tris pH=8.0), to reach a NaCl concentration of 25 mM, and incubated with ULP-1 SUMO protease (SAE0067-2500UN, Sigma-Aldrich) (20 U·mg^{-1} SUMO-XCL1, 16 hours, RT) on an end-over-end shaker. The reaction was subsequently incubated with prewashed Ni-NTA resin to remove 6×His SUMO and ULP-1 (1 hour, RT), and transferred to a disposable chromatography column. Flow through was collected and concentrated on a 3 kDa spin filter (cycles of 10 min, 4°C, 3 000 g) (UFC800324, Merck-Millipore). Concentration was measured on a Nanodrop 2000 (ND-2000C, ThermoFisher) (MW=12 100 Da, ε_{280nm}= 8 730 M^{-1}·cm^{-1}), and aliquots were stored at −80°C. Production steps, and final product purity were assessed on a 15% sodium-dodecyl-sulfate polyacrylamide gel electrophoresis (SDS-PAGE) using SYPRO Ruby Protein Gel Stain (S12000, Thermo Fisher Scientific). Refolding efficacy was measured by denaturing XCL1 with 20 µM beta-mercaptoethanol and comparing retention times by reverse phase HPLC (C_{18} column). 6×His-SUMO-XCL1(CC3)-LPETG-FLAG sequence is available in table 1.

Sortase production

Sortase was produced in BL21(DE3) *E. coli* as reported.[21] Briefly, chemically competent BL21(DE3) were transformed by heat shock, and grown overnight (30°C, 220 rpm) in selective media (LB + 50 µg·mL^{-1} kanamycin). The next day, selective media was inoculated at OD_{600}~0.05, and bacteria were grown (37°C, 220 rpm) to an OD_{600}~0.6, and induced with IPTG at a final concentration of 1 mM (16 hours, 25°C, 220 rpm). Bacteria were collected by centrifugation, pellets were washed with (50 mM Tris pH=7.5, 150 mM NaCl), and frozen at −20°C overnight. Pellets were thawed on ice and resuspended in lysis buffer (50 mM Tris pH=7.5, 150 mM NaCl, 10 mM imidazole, 20 µg·mL^{-1} of protease inhibitor cocktail, 10% (v/v) glycerol). Suspension was lysed by sonication on ice (3×30 s, 25% amplitude), and centrifuged (30 min, 4°C, 8 600 g). Supernatant was collected, and protein was isolated using Ni-NTA resin (1 hour, 4°C). Resin was transferred to a disposable column and washed with 100 CV of ice-cold wash buffer (50 mM Tris pH=7.5, 150 mM NaCl, 10 mM imidazole). Protein was eluted using 2×4 CV ice-cold elution buffer (50 mM Tris pH=7.5, 150 mM NaCl, 500 mM imidazole, 10% (v/v) glycerol), and washed by ultracentrifugation (cycles of 10 min, 4°C, 3 000 g) on a 3 kDa filter (UFC900324, Merck-Millipore). Protein concentration was measured on a Nanodrop 2000 (MW=17 752 Da, ε_{280nm}=14 565 M^{-1}·cm^{-1}), and sortase was stored at −80°C in sortase buffer (50 mM Tris pH=7.5, 150 mM NaCl) supplemented with 10% (v/v) glycerol. Protein purity was assessed on a 12% SDS-PAGE. Protein was stored at −80°C.

sdAb production

A single-domain antibody (sdAb) against BDCA-2 was identified and characterized in house. BL21 (DE3) *E. coli* bacteria were transformed by heat shock and grown (16 hours, 30°C) in 50 mL of LB + 100 µg·mL^{-1} ampicillin. The next day, bacteria were diluted in fresh selective media, and grown (37°C, 220 rpm) to reach OD_{600}~0.6. sdAb production was induced with IPTG at a final concentration of 1 mM, and bacteria were cultured

Table 1 Amino acid sequence of 6×His-SUMO-XCL1(CC3)-LPETGG-FLAG

Feature	AA sequence
N-terminal histag	MGSSHHHHHH
SUMO solubility domain ↓: ULP-1 cleavage site	SSGLVPRGSHMSDSEVNQEAKPEVKPEVKPETHINLKVSDGSSEIFFKIKKTTPLRRLMEAFAKRQGKEMDSLR FLYDGIRIQADQTPEDLDMEDNDIIEAHREQIGG↓
XCL1 V21C/V59C	VGSEVSDKRTCVSLTTQRLPCSRIKTYTITEGSLRAVIFITKRGLKVCADPQATWVRDCVRSMDRKSNTRNNMIQ TKPTGTQQSTNTAVTLT
G4S – sortagging site ↓: sortase cleavage site	GGGGGSLPET↓GG
FLAG tag	DYKDDDDK

(16 hours, 30°C). Bacteria were pelleted (30 min, 4°C, 3 000 g), and resuspended in 1×TES (50 mM Tris, 500 mM sucrose, 0.65 mM EDTA) (20 mL per L of original culture) (1 hour, 4°C) on a roller shaker. Osmotic shock was performed by diluting suspension with 0.25×TES (80 mL per L of original culture) (16 hours, 4°C). Suspension was spun (25 min, 4°C, 8 600 g) and supernatant (periplasmic extract) was collected. Periplasmic fraction was incubated with an appropriate amount of pre-washed Ni-NTA resin (1 hour, 4°C). Resin was transferred to a disposable column and washed with 100 CV ice-cold wash buffer (50 mM Tris pH=8.0, 150 mM NaCl, 10 mM imidazole). Protein was eluted with 2×4 CV ice-cold elution buffer (50 mM Tris pH=8.0, 150 mM NaCl, 500 mM imidazole). Buffer exchange to sortase buffer (50 mM Tris pH=7.5, 150 mM NaCl) was performed by spin filtration (cycles of 10 min, 4°C, 3 000 g). Protein concentration was measured using a Nanodrop 2000 (MW=15 600 Da, ε_{280nm}= 21 550 $M^{-1}\cdot cm^{-1}$)), and purity was assessed by SDS-PAGE. Protein was stored at −80°C.

Peptide synthesis

(H-GGG-CK(FITC)-NH_2) and (H-GGG-K(N_3)-NH_2) synthesis was described previously. For (GGG-K(N_3) FRSLLMWITQ(Abu)) and (GGG-K(N_3)FRYLEPG-PVTA) synthesis, 25 mL polypropylene syringes with a porous disc were used for solid-phase peptide synthesis. In short, 2-chlorotrityl chloride resin (100–200 mesh) was used with a loading of 1.5 $mmol\cdot g^{-1}$ and peptide couplings were performed with a mixture of Fmoc-AA-OH/DIPCDI/Oxyma Pure (three equiv. each). After cleavage with TFA:TIS:ddH_2O (95:2.5:2.5), the peptide was precipitated in Et2O, lyophilized, and finally purified using a preparative-HPLC-ESI system (Waters) using a C_{18} reverse phase column, and gradient from 80:20 to 55:45 ddH_2O:acetonitrile (ACN) in 15 min. Peptide masses were initially predicted by ChemDraw Professional 15.0 (PerkinElmer, Massachusetts, USA) and compared with acquired masses after LC-MS measurements. (GGG-K(N_3) FRRLSSCVPVA) and (GGG-K(N_3)FRFLIIWQNTM) were commercially synthesized by Peptide Specialty Laboratories GmbH (Heidelberg, DE). MS analysis of the antigen-containing peptides is available in online supplemental figure S2A.

GGG-K(N_3)-X conjugation to polyethylene glycol-DBCO

(GGG-K(N_3)-FR-X) was dissolved at 1 $mg\cdot mL^{-1}$ in 1:1 (v/v) ACN:ddH_2O. DBCO-polyethylene glycol (PEG5k) (three equiv.) were added, and reaction was incubated (3 hours, 37°C) on an end-over-end shaker. Because of cross-reactivity of the thiol in the active site of the sortase, free DBCO groups were quenched by addition of NaN_3 (two equiv.) (overnight, RT). Mixture was diluted with ddH_2O to reduce ACN content to 15% (v/v) and lyophilized. Peptide was dissolved at 5 mM in DMSO and used in site-specific modification reactions. Conversion rate was assessed by HPLC.

Analytical HPLC

Lyophilized peptides and XCL1 were dissolved at 1 $mg\cdot mL^{-1}$ in ACN:ddH2O (1:1 v/v) supplemented with 0.01% TFA, and analytical HPLC was carried out on Shimadzu instrument composed of a CBM-20A communication Bus module, DGU-20AS degasser, 2 LC20AD pumps, SIL-20AC autosampler, SPD-M20A diode array detector and CTO-20AC column oven. For XCL1(CC3) and S7Abu peptides, a linear gradient from 5% to 95% of ACN (+0.036% TFA) into ddH_2O (+0.045% TFA) were run at flow rate of 1 $mL\cdot min^{-1}$ over 15 min. For Y7A, R7A and F7M peptides, a linear gradient from 5% to 95% of ACN (+0.01% TFA) into ddH_2O (+0.01% TFA) were run at flow rate of 1 $mL\cdot min^{-1}$ over 37 min. XSelect Peptide CSHTM C18, 130 Å, 3.5 µm, 4.6 mm × 100 mm (Waters) column was used for the analysis. Chromatographic peak area was determined at λ=220 nm.

MALDI-TOF

(*m/z*) of the (GGG-K(N_3)-FR-SLLMWITQ(Abu)) peptide before and after PEGylation was analyzed on Bruker Microflex LRF MALDI-TOF equipment. Samples were analyzed within a concentration range of 0.3–0.5 $mg\cdot mL^{-1}$ in ACN:ddH_2O (1:1 v/v), using 1 µL of matrix-sample-matrix sown on the MALDI plate. Matrix: Sinapic acid (trans-3,5-dimethoxy-4-hydroxycinnamic acid) (D7927, Sigma Aldrich) at 10 $mg\cdot mL^{-1}$ in ACN:ddH_2O (1:1 v/v) + 0.1% TFA.

Troubleshooting NY-ESO conjugation

We aimed at improving the stability of XCL1-K(N_3)-S7Abu by modifying several conditions in the workflow (table 2). We notably modified the reaction and purification buffer, which did not change the outcome. We additionally kept the SUMO solubility domain during XCL1 labeling and aimed at performing ULP1 cleavage afterwards to improve overall solubility during the purification, but the product likewise aggregated before ULP1 digestion.

Sortagging and purification

Site-specific chemoenzymatic transpeptidation was achieved by incubating XCL1 (final concentration 5 µM) or sdAb (final concentration 20 µM) with 3M sortase A (0.75 equiv.) or 5M sortase A (0.4 equiv.), (H-GGG-X) peptide (25 equiv.), $CaCl_2$ (10 mM), DMSO (10% v/v), in sortase buffer (50 mM Tris pH=7.5, 150 mM NaCl). Reactions were incubated (1 hour, 37°C, 400 rpm for 3M sortase or 2 hours, 4°C, 400 rpm for 5M sortase) and transferred to an appropriate volume of prewashed Ni-NTA resin (30 min, 4°C) on an end-over-end shaker. Reaction was spun over a 100 µm filter to remove Ni-NTA resin, flow-through was collected, and spun (10 min, 4°C, 10 000 g) to remove eventual aggregates. Subsequent protein purification workflows are described below. After purification, proteins were concentrated on a 0.5 mL 3 kDa filter (cycles of 10 min, 4°C, 10 000 g) and purity was controlled by SDS-PAGE.

Table 2 Troubleshooting of site-specific GGG-K(N_3)-S7Abu conjugation to XCL1

Troubleshooting	Outcome	Conclusion
Lower equivalents of peptide in reaction	Selective aggregation of sortagged product	Insolubility of XCL1(CC3)-K(N_3)-S7Abu in sortase buffer
Adding 10% final (v/v) glycerol to reaction[36] (interacts with large hydrophobic patches and improves solubility)	Selective aggregation of sortagged product	10% (v/v) glycerol did not improve solubility of XCL1(CC3)-K(N_3)-S7Abu
Addition of 10 mM L-arginine·HCl[37 51]	Selective aggregation of sortagged product	L-arginine·HCl did not prevent aggregation of insoluble XCL1(CC3)-K(N_3)-S7Abu
Immobilization of sortase on NiNTA resin	Selective aggregation of sortagged product	Sortase immobilization did not prevent aggregation of product
SUMO solubility domain removal after XCL1 modification	Selective aggregation of sortagged product	Presence of the solubility domain did not enable isolation of SUMO-XCL1(CC3)-K(N_3)-S7Abu
PEGylation of peptide[38 39 52] at K(N_3)	Solubility of peptide and product in sortase buffer	Purification of XCL1(CC3)-K(PEG5k)-S7Abu possible on large scale

For conjugation to (H-GGG-CK(FITC)-NH_2), product was purified by fast protein liquid chromatography (FPLC, NGC Quest, BioRad) on an ENrich SEC70 10×300 column (7801070, BioRad) in sortase buffer.

For conjugation to Cy5.5, XCL1 or sdAb were site-specifically labeled with (H-GGG-K(N_3)-NH_2) and purified by FPLC to remove peptide excess. XCL1-K(N_3) and sdAb-K(N_3) were subsequently reacted with DBCO-Cy5.5 (3 equiv.) (CLK-1046, Jena BioSciences) (16 hours, RT) on an end-over-end shaker. Peptide excess was removed by running the reaction through a PD-10 desalting column (17085101, Cytiva).

For conjugation to (GGG-K(PEG)FR-X), product was loaded onto a strong cation exchange column (HiTrap SP FF, 17505401, Cytiva), and eluted with a gradient of 50 mM Tris+150 mM – 1 M NaCl. pH of the Tris buffer was adjusted to 7.5 at RT (XCL1 V21C/V59C), or 5.1 at RT (sdAb) to accommodate for the isoelectric point of the protein. Fractions were collected and NaCl concentration was adjusted by diluting with 50 mM Tris to 150 mM. If necessary, protein was incubated with anti-FLAG resin (16 hours, RT) (L00432, Genscript) to remove unreacted XCL1. Protein was concentrated on 3 kDa spin filters (cycles of 10 min, 4°C, 8 600 g), buffer exchange to sortase buffer (50 mM Tris pH=7.5, 150 mM NaCl) was performed, and protein was incubated with a Pierce endotoxin removal column (16 hours, 4°C) (88274, ThermoFisher). Protein was eluted (2 min, 4°C, 3 000 g), further concentrated on a 0.5 mL 3 kDa filter (cycles of 10 min, 4°C, 8 600 g) to reach a final concentration of 1–3 mg·mL^{-1}, and aliquoted at −80°C until further use. Endotoxin levels were confirmed below detection levels by chromogenic Limulus amebocyte lysate test, performed by the Radboudumc pharmacy (Nijmegen, NL).

PBMC isolation

Buffycoats or apheresis material from HLA-A*02:01$^+$ donors were obtained from Sanquin (Nijmegen, NL). PBMC suspension was diluted to 300 mL with RT dilution buffer (PBS + 2 mM EDTA) and split over 10×50 mL conical tubes. 10 mL of Lymphoprep (07851, Stemcell) was carefully pipetted underneath, and cells were spun (20 min, RT, 2 100 rpm, brake (2,0)). After centrifugation, peripheral blood mononuclear cells (PBMCs) were carefully collected with a 5 mL pipet and transferred to new 50 mL tubes. Cells were diluted up to 50 mL with dilution buffer and spun (10 min, RT, 1 800 rpm). Pellets were washed with 40 mL ice-cold wash buffer (PBS + 1% human serum albumin (HSA) + 2 mM EDTA) three times (5 min, 4°C, 1 500 rpm), and split over two tubes. Cells were washed one time with ice-cold PBS, and erythrocytes lysed with 10 mL of ACK lysis buffer (150 mM NH_4Cl, 10 mM $KHCO_3$, 0.1 mM Na_2EDTA, pH=7.2–7.4) (5 min, RT). Wash buffer was added to 50 mL, cells were spun (5 min, 4°C, 1 500 rpm) and resuspended in 50 mL wash buffer. Cells were counted using Türks reagent.

CD8$^+$ T cell isolation and transfection

From each donor, 3–5×10^8 PBMCs (apheresis) or 1–2×10^8 PBMCs (buffycoats) were used to obtain CD8$^+$ T cells by negative magnetic isolation (130-096-495, Miltenyi Biotech), according to the manufacturer's instructions. Cells were counted and washed with a large volume of RT PBS. 1–1.5×10^7 CD8$^+$ T cells were resuspended in 250 µL of RT red phenol-free serum-free TheraPEAK™ X-VIVO™-15 (BEBP02-061Q, Lonza). 10 µg of RNA coding for the α and β chains of the TCR recognizing the S7C epitope of NY-ESO-1 presented on HLA-A*02:01 (NY-ESO (157-165)) was thawed on ice and added to the cell suspension. Cells were transferred to the electroporation cuvette (1652088, BioRad), and transfected using a Gene Pulser Xcell electroporation system (1652661, BioRad) using the following settings: square wave, 500 V, 3 ms, 1 pulse, 4 mm. Cells were carefully transferred to a 15 mL tube containing 1 mL of pre-warmed RPMI + 4% human serum (HS), and left to recover (37°C, at least 2 hours) until further processing. Cells were washed with a large volume of PBS and resuspended in 200 µL PBS+2% fetal bovine serum (FBS), to which 200 µL PBS+10 µM Cell Trace Far Red (CTFR) was added. Cells were incubated (37°C, 20 min), with gentle shaking after 10 min. 2 mL of pre-warmed FBS were added, and cells were further

incubated (37°C, 10 min) to quench CTFR. Cells were spun down (5 min, 4°C, 1 500 rpm), washed with X-VIVO™-15 (BE02-060Q, Lonza) + 2% HS, and counted (expected yield is 5–8×10^6 cells). Cells were resuspended in X-VIVO-15 + 2% HS for further use. TCR expression was analyzed the next day by flow cytometry using an anti-mouse TCR antibody (H57-597, BV421, BioLegend).

Isolation of cDC1s from HLA-A*02:01$^+$ PBMCs

From each donor, the rest of PBMCs (typically 2–4×10^9 cells for apheresis, or 4–6×10^8 cells for buffycoats) was used to proceed to cDC1 isolation. Cell pellet was resuspended in 1 µL per 1×10^6 cells of microbeads against CD19 (130-050-301, Miltenyi Biotech), CD3 (130-050-101, Miltenyi Biotech), CD14 (130-050-201, Miltenyi Biotech), CD56 (130-050-401, Miltenyi Biotech) and 1 µL per 1×10^6 cells of FcR block (130-059-901, Miltenyi Biotech). Cell suspension was incubated (30 min, 4°C) on a roller shaker. Cells were diluted with a large volume of wash buffer (PBS + 1% HSA + 2 mM EDTA) and spun (5 min, 4°C, 1 500 rpm). Cells were resuspended in 1 mL per 1×10^8 cells, and ran over prewashed LS columns (130-042-401, Miltenyi, 1 LS per 1×10^8 cells). Columns were washed with 3×3 mL of wash buffer. Negative fraction was collected, and cells were counted, spun (5 min, 4 C, 1 500 rpm), resuspended in 1 mL per 1×10^8 cells, and ran over pre-washed LD columns (130-042-901, Miltenyi, 1 LD per 1×10^8 cells). Columns were washed with 3×3 mL of wash buffer. Negative fraction was collected, and cells were pooled, counted (expected yield after LS and LD is 1–5% of PBMCs), and spun (5 min, 4°C, 1 500 rpm). Cells were resuspended in 2 µL wash buffer per 1×10^6 cells, and 1 µL anti-CD1c-biotin (130-119-475, Miltenyi Biotech) per 1×10^6 cells for 15 min at 4°C, with gentle shaking every 5 min. Cells were washed with a large volume of cold wash buffer, spun (5 min, 4°C, 1 500 rpm), and incubated with 2 µL of anti-biotin microbeads for another 15 min. Cells were washed, and resuspended in 1 mL wash buffer, and ran through a prewashed LS column. Column was washed with 3×3 mL wash buffer, and eluted with 1 mL wash buffer, and positively isolated cDC2s were directly ran over a pre-washed MS column (130-042-201, Miltenyi). Column was washed with 2×1 mL wash buffer and eluted with 1 mL wash buffer. cDC2s were immediately counted and resuspended in X-VIVO-15 + 2% HS at 1×10^6 cells·mL^{-1}. Negative fraction (cDC1-containing) was further processed by resuspending in 2 µL wash buffer per 1×10^6 cells, and 1 µL anti-BDCA-3 microbeads (130-090-512, Miltenyi Biotech) per 1×10^6 cells (15 min, 4°C), with gentle shaking every 5 min. Cells were washed with a large volume of wash buffer, and spun (5 min, 4°C, 1 500 rpm). Cells were resuspended in 1 mL wash buffer and ran over a prewashed LS column. Column was washed with 3×3 mL wash buffer, eluted with 1 mL wash buffer, and positively isolated cDC1s were directly ran over a pre-washed MS column (130-042-201, Miltenyi). Column was washed with 2×1 mL wash buffer and eluted with 1 mL wash buffer. Cells were immediately counted, and resuspended in X-VIVO-15 + 2% HS at 1×10^6 cells·mL^{-1}. The unlabeled fraction (CD3$^-$CD14$^-$CD19$^-$CD56$^-$CD1c$^-$CD141$^-$) was kept for some experiments.

cDC1 / CD8$^+$ T cell activation assay

cDC1s from HLA-A*02:01$^+$ healthy donors were isolated. For apheresis material, 10 000 cDC1s were seeded in 50 µL in a round bottom 96-well plate (3799, Corning) and treated with XCL1-K(PEG)-S7Abu or sdAb-K(PEG)-S7Abu (1 µM or 0.1 µM) for 3 hours, in a final volume of 100 µL X-VIVO-15 + 2% HS + 1 µg·mL^{-1} poly(I:C) (tlrl-picw, Invivogen). After 3 hours, 100 µL X-VIVO-15 + 2% HS was added, and cells were spun down. Supernatant was carefully pipetted off, and cells were resuspended in 100 µL X-VIVO-15 + 2% HS + 0.6 µg·mL^{-1} poly(I:C). 50 000 TCR-transfected CD8$^+$ T cells were added in 100 µL, and cells were incubated for 120 hours. 50 µL supernatant was harvested after 24 hours. Division index was calculated by the formula $DI = \frac{\sum_0^i i* \frac{N_i}{2^i}}{\sum_0^i \frac{N_i}{2^i}}$, where i is the division cycle number, and N_i the percentage of live CD8$^+$ T cells in that cell cycle.

For buffycoat material, 5 000 cDC1s, 5 000 cDC2s or 50 000 cells from the negative fraction were plated in various combinations with 0.1 µM XCL1-K(PEG)-S7Abu for 3 hours in a final volume of 100 µL X-VIVO-15+2% HS + 1 µg·mL^{-1} poly(I:C). After 3 hours, 100 µL X-VIVO-15 + 2% HS was added, and cells were spun down. Supernatant was carefully pipetted off, and cells were resuspended in 100 µL X-VIVO-15 + 2% HS + 0.6 µg·mL^{-1} poly(I:C). 50 000 TCR-transfected CD8$^+$ T cells were added in 100 µL, and cells were incubated for 120 hours.

In vitro chemotaxis assay

Apheresis material was obtained from healthy donors as part of an ongoing study, and cDC1s were isolated as described. 50 000 freshly isolated primary cDC1s were placed in 100 µL X-Vivo-15 + 2% HS in the top compartment of a 5 µm HTS transwell (3388, Corning). Lower compartment was filled with 200 µL X-Vivo-15 + 2% HS, eventually supplemented with 10 ng·mL^{-1} recombinant XCL1 (758002, BioLegend), 10 ng·mL^{-1} in house-generated XCL1(CC3), or 10 ng·mL^{-1} XCL1(CC3)-K(PEG)-S7Abu, and cells were incubated (37°C, 15 hours). Cells migrating toward the lower compartment were directly harvested and counted using a MACSQuant (Miltenyi). XCL1-mediated chemotaxis was calculated by the formula: $\%\ \text{migration} = \frac{\%\ \text{migration in condition}}{\%\ \text{migration to rhXCL1}}$.

Flow cytometry

Stainings were performed in 50 µL in 96-well plates. Live/death staining was performed with fixable eFluor506 viability dye (1:2000, 65-0866-14, ThermoFisher) in PBS (30 min, RT). Antibody stainings were performed in PBA (PBS + 5% FBS + 0.01% NaN_3) (30 min, 4°C). DC purity was assessed by antibodies against CD141 (1:10, APC, AD5-14H12, 130-113-314, Miltenyi) and XCR1 (1:10, PE, S15046E, 372604, BioLegend), and T cell phenotype was

assessed by antibodies against CD25 (1:100, AF488, BC96, 302616, BioLegend), CD127 (1:100, PE/Cy7, A019D5, 351320, BioLegend), CD137 (1:100, PE, 4B4-1, 555956, BD Pharmigen), CD279 (1:100, BV421, EH12.2H7, 329920, BioLegend), and TIGIT (1:100, BB700, 741182, 747846, BioLegend). Cells were washed 2× with PBA before acquisition on a FACSLyric (BD).

ELISA

ELISA was performed for IFNγ and IL-2 using uncoated kits (respectively 88-7316-88 and 88-7025-88, ThermoFisher) following manufacturer's instructions. Briefly, plates were coated with 100 µL capture antibody diluted in coating buffer (50 mM Na_2CO_3/$NaHCO_3$, pH=9.6) (16 hours, 4°C). Plates were washed 3× with wash buffer (PBS + 0.05% Tween-20), blocked with 200 µL ELISA diluent reagent (1 hour, RT), and washed 1×. Supernatants were diluted in ELISA diluent reagent (1:50 for IFNγ and 1:10 for IL-2), and 100 µL were incubated with the capture antibody (2 hours, RT). Plates were washed 5× and incubated with 100 µL diluted detection antibody (1 hour, RT). Plates were washed 5× and incubated with 100 µL diluted streptavidin-HRP (30 min, RT). Plates were washed 7× and incubated with 100 µL TMB. Reactions were developed in the dark and stopped with 100 µL 2 M H_2SO_4. Absorbance was measured at λ=450 nm on an iMark microplate reader (1681130, Bio-Rad). Standard was prepared in duplicate and used to perform quantification using a Four parameter logistic (4PL) modeling (available at: https://www.arigobio.com/elisa-analysis).

Microscopy

Freshly isolated cDC1s were resuspended in PBA and stained with either XCL1(CC3)-Cy5.5 or sdAb-Cy5.5 (10 µg·mL^{-1}, 30 min, 4°C). Cells were washed 1× with 100 µL PBA and 1× with 100 µL PBS. Cells were resuspended in 100 µL 4% paraformaldehyde (PFA), and fixed (30 min, 4°C). In the meantime, 12 mm circular confocal slides (72 230–01, 1 ½, Electron Microscopy Sciences) were placed on parafilm, cleaned with 100% ethanol (1 min), and washed 2× with 100 µL PBS. Slides were coated with ±100 µL of 10 µg·mL^{-1} poly-L-lysine in ddH_2O (25 min, RT). Fixed cDC1s were spun (10 min, RT, 2 000 rpm), and washed 2× with 100 µL of RT PBS. Slides were washed 1× with PBS and 40 µL of cell suspension was carefully pipeted onto the coverslip (30 min, RT, protected from light). Finally, slides were mounted face down on 4 µL embedding medium (24% (w/v) glycerol, 9.6% (w/v) Mowiol 4–88, 1.5 µg·mL^{-1} DAPI, 0.1 M Tris pH=8.5), left to polymerize in the dark at RT overnight, and further stored at −20°C. Fluorescence was acquired on a LSM900 (Zeiss, Jena, DE).

RESULTS

XCL1(CC3) can be site-specifically labeled without disrupting binding to XCR1

In order to site-specifically modify XCL1(CC3), we genetically fused it to a *N*-terminal His-tagged SUMO solubility tag and a C-terminal FLAG-tagged LPETGG sortag motif (figure 1A). After production and refolding, we isolated XCL1(CC3)-LPETGG-FLAG by nickel affinity purification (figure 1B). This typically yielded ~5–10 mg XCL1(CC3) per liter of starting culture, with a refolding efficacy over 85%, as analyzed by HPLC (online supplemental figure S1A). To confirm that XCL1(CC3) was able to retain its binding specificity following site-directed modification, we subjected XCL1(CC3)-LPETGG-FLAG to site-specific conjugation to two small peptides (H-GGGCK(FITC)-NH_2) (referred to as FITC) and (H-GGG-K(N_3)-NH_2) (referred to as N_3). We were able to isolate XCL1(CC3)-FITC and XCL1(CC3)-N_3 with a yield of ~45%. XCL1(CC3)-N_3 was further reacted with DBCO-Cy5.5 to generate XCL1-Cy5.5 (figure 1C, online supplemental figures S1B,D). To confirm binding capacity and specificity, we incubated a mixture of freshly isolated cDC2s ($CD1c^+CD141^-XCR1^-$) and cDC1s ($CD14^+XCR1^+$), with either a commercial anti-XCR1 antibody or XCL1(CC3)-FITC. As analyzed by flow cytometry (figure 1D and online supplemental figure S1C), XCL1(CC3)-FITC specifically identified a subpopulation of cDC1s (~60% of cDC1s), similarly to the commercial antibody. Moreover, XCR1 expression on primary cDC1s could be visualized by confocal microscopy using XCL1(CC3)-Cy5.5 (figure 1E). Hence, introduction of a LPETGG motif at the C-terminus of XCL1(CC3) did not impair folding, and the engineered chemokine could be modified site-specifically with fluorescent peptides, while retaining its binding capacity.

Poor solubility of tumor antigen prevents conjugation to XCL1

After confirming that XCL1(CC3)-LPETGG-FLAG could be modified while retaining XCR1 binding capacity, we set out to generate a construct able to deliver tumor antigens to cDC1s. To this end, we synthesized a peptide containing a triglycine motif, an azido-lysine as clickable handle, a FR- dipeptide motif to promote cross-presentation by biasing proteasomal cleavage,[27] followed by S7Abu, ((GGG-K(N_3)FRSLLMWITQ(Abu)), referred to as K(N_3)-S7Abu). After site-specific labeling of XCL1(CC3)-LPETGG-FLAG, we detected formation of XCL1(CC3)-K(N_3)-S7Abu with minimal hydrolysis product (XCL1-H) (online supplemental figure S1E). However, the product could not be purified (online supplemental figure S2B), suggesting that XCL1-K(N_3)-S7Abu was not stable in solution. Further analysis indicated that the product was entirely present in aggregates formed during the reaction (online supplemental figure S2C). Sortase-mediated transpeptidation exchanged a solubilizing His-tag for an extremely hydrophobic S7Abu epitope, likely causing this aggregation.

PEGylation of tumor antigen allows conjugation of S7Abu to XCL1(CC3)

As peptide conjugation appeared to induce aggregation of XCL1(CC3)-K(N_3)-S7Abu, we decided to use the azido-lysine to introduce a 5 kDa polyethylene glycol (PEG5k) chain via copper free strain-promoted azide–alkyne cycloaddition (SPAAC) (figure 2A). We performed a SPAAC reaction of (K(N_3)-S7Abu) with a three-fold excess

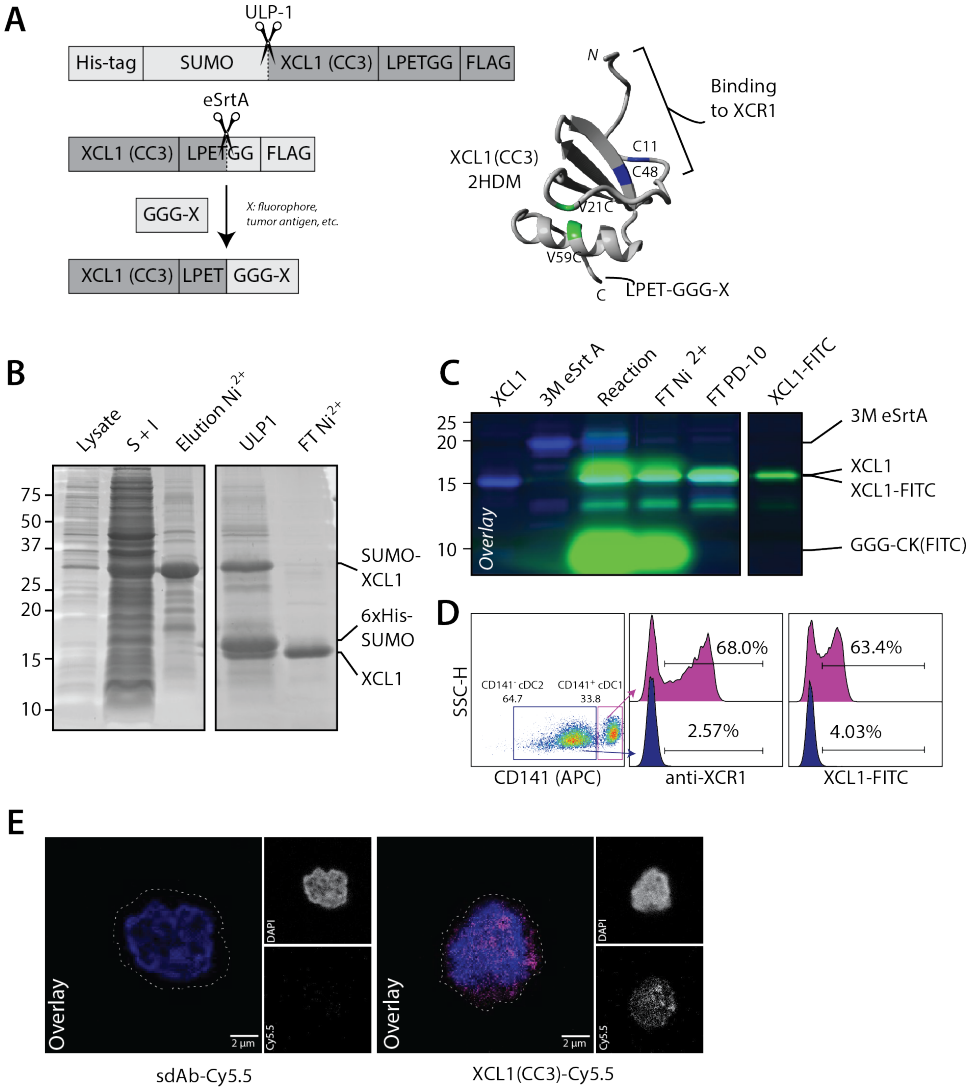

Figure 1 XCL1(CC3)-LPETG retains binding specificity to XCR1 after site-specific labeling with a small fluorophore. (**A**) Representation of 6×His-SUMO-XCL1-LPETGG-FLAG produced in BL21(DE3), site-specific labeling via sortase-mediated transpeptidation, and structure of XCL1(CC3) after purification and refolding. V21C and V59C point mutations stabilizing the α-β chemokine fold are highlighted in green, and two cysteine residues C11 and C48 present in the native XCL1 are highlighted in blue. Adapted from 2HDM structure[20] and modeled in YASARA. (**B**) Production of XCL1(CC3) in BL21(DE3) *Escherichia coli*. ~30 kDa 6×His-SUMO-XCL1(CC3)-LPETGG-FLAG is present in bacterial lysate (lane 1) and enriched by pooling the soluble and insoluble fractions (S+I, Lane 2). 6×His-SUMO-XCL1 is eluted (lane 3) after nickel affinity purification, and solubility tag digested (ULP1, lane 4). XCL1(CC3) is isolated after a second nickel purification (FT Ni^{2+}, Lane 5) with high purity. (**C**) Overlay of Sypro staining and 488 nm in-gel fluorescence. Site-specific labeling of XCL1(CC3) (lane 1) with 3M eSrtA (lane 2) and GGGCK(FITC). After reaction (lane 3), XCL1(CC3)-FITC is purified by nickel affinity purification (FT Ni^{2+}, Lane 4), FITC excess removed by PD-10 desalting (Lane 5) and pure product is obtained after concentration (Lane 6). (**D**) Commercial anti-XCR1-PE and XCL1(CC3)-FITC identify a comparable subpopulation of ~60% $CD141^+$ cDC1s without staining $CD141^-$ cDC2s, confirming that XCL1(CC3)-FITC specifically binds to XCR1. (**E**) Surface staining of cDC1s with 10 µg·mL^{-1} XCL1(CC3)-Cy5.5 or sdAb-Cy5.5 at 4°C for 30 min before fixation shows specificity of XCL1(CC3) for XCR1, as imaged by confocal microscopy. cDC1, conventional dendritic cell type 1.

of DBCO-PEG5k. Reaction completion was confirmed by HPLC (online supplemental figure S2E) and Matrix-assisted laser desorption/ionization-Time-of-Flight (MALDI-TOF) (online supplemental figure S2D). Excess DBCO-PEG5k was capped by addition of NaN_3, followed by site-specific conjugation of (GGG-K(PEG5k)FR-S7Abu) (K(PEG)-S7Abu) to XCL1. We observed formation of XCL1(CC3)-K(PEG)-S7Abu, which we could purify by cation exchange chromatography with an isolated yield above 40%, and over 75% purity as seen by SDS-PAGE (figure 2B). A competitive flow cytometry-based binding assay performed with freshly isolated cDC1s by flow cytometry revealed that presence of XCL1(CC3)-K(PEG)-S7Abu was able to prevent binding of an anti-XCR1 commercial antibody (figure 2C). Thus, modification and PEGylation of the chemokine did not impair its binding capacity. Importantly, XCL1(CC3)-K(PEG)-S7Abu also had similar chemotactic activity compared to commercial XCL1, and

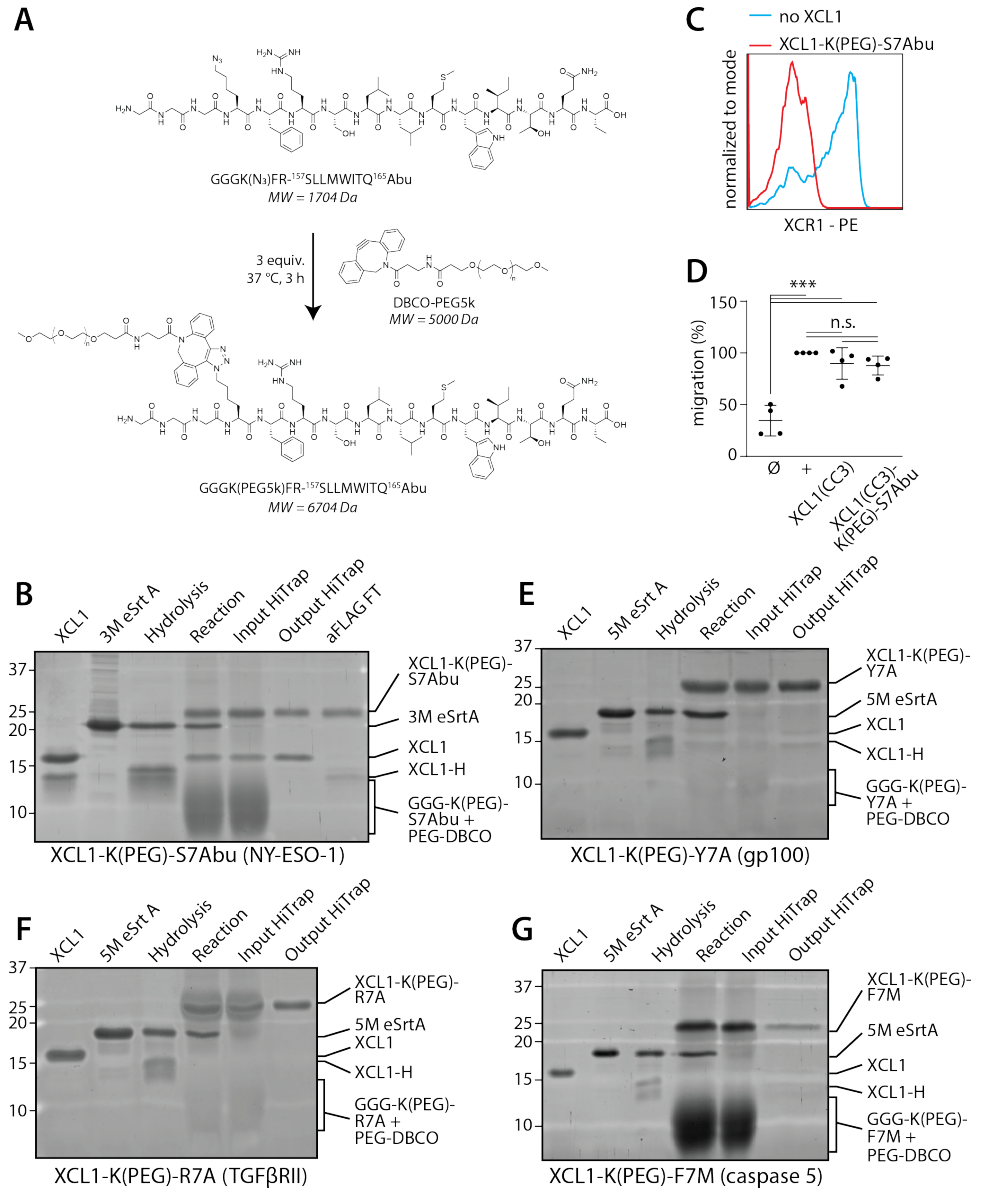

Figure 2 PEGylation of GGG-K(N_3)-S7Abu enables its conjugation to XCL1(CC3). (**A**) Site-specific PEGylation of GGG-K(N_3)-S7Abu with DBCO-PEG5k. (**B**) 3M sortase-mediated site-specific labeling of XCL1(CC3) (lane 1) with GGG-K(PEG)-S7Abu allows product formation (lane 4). Sortase is removed by incubation with Ni-NTA resin (lane 5), excess of nucleophile and PEG5k is removed after cation exchange (lane 6), and unreacted XCL1(CC3) removed by incubation with anti-FLAG beads, allowing isolation of pure XCL1(CC3)-K(PEG)-S7Abu (lane 7). 3M eSrtA (lane 2) activity is confirmed by hydrolysis of XCL1(CC3) in absence of peptide (lane 3). Densitometry was performed to calculate the concentration of XCL1(CC3)-K(PEG)-S7Abu used in cell experiments. (**C**) Incubation of XCR1-expressing cDC1s with anti-XCR1 in presence or absence of XCL1(CC3)-K(PEG)-S7Abu shows that the PEGylated vaccine retains binding to XCR1. (**D**) cDC1 migration towards media (Ø), 10 ng·mL-1 rhXCL1 (+, BioLegend), XCL1(CC3), and XCL1(CC3)-K(PEG)-S7Abu, shows that modification of XCL1 does not impair its chemotactic activity. N=4 independent donors, normalized to rhXCL1. One-way ANOVA, ***p<0.001. (**E-G**) 5M sortase-mediated site-specific labeling of XCL1(CC3) (lane 1) with GGG-K(PEG)-Y7A (gp100) (E), GGG-K(PEG)-R7A (TGFβRII) (F) and GGG-K(PEG)-F7M (caspase 5) (G) allows product formation (lane 4). Sortase is removed by incubation with Ni-NTA resin (lane 5), and excess of nucleophile and PEG5k is removed after cation exchange (lane 6), allowing isolation of pure XCL1(CC3)-K(PEG)-S7Abu (lane 6). 5M eSrtA (lane 2) activity is confirmed by hydrolysis of XCL1(CC3) in absence of peptide (lane 3). ANOVA, analysis of variance.

unlabeled XCL1(CC3) (figure 2D), demonstrating that modification of the chemokine did not affect its functionality. In lieu of an isotype control, we generated a non-specific vaccine by modifying an in-house-generated single domain antibody (sdAb) directed against BDCA-2 (CD303), a plasmacytoid DC marker, and could isolate sdAb-K(PEG)-S7Abu using a similar method with comparable yields (online supplemental figure S2F).

To demonstrate the applicability of the platform, we generated XCL1(CC3)-antigen constructs using distinct tumor epitopes. We selected HLA-A*02:01 epitopes of the TAA gp100 (^{280}YLEPGPVT^{288}A, in short Y7A), and of two

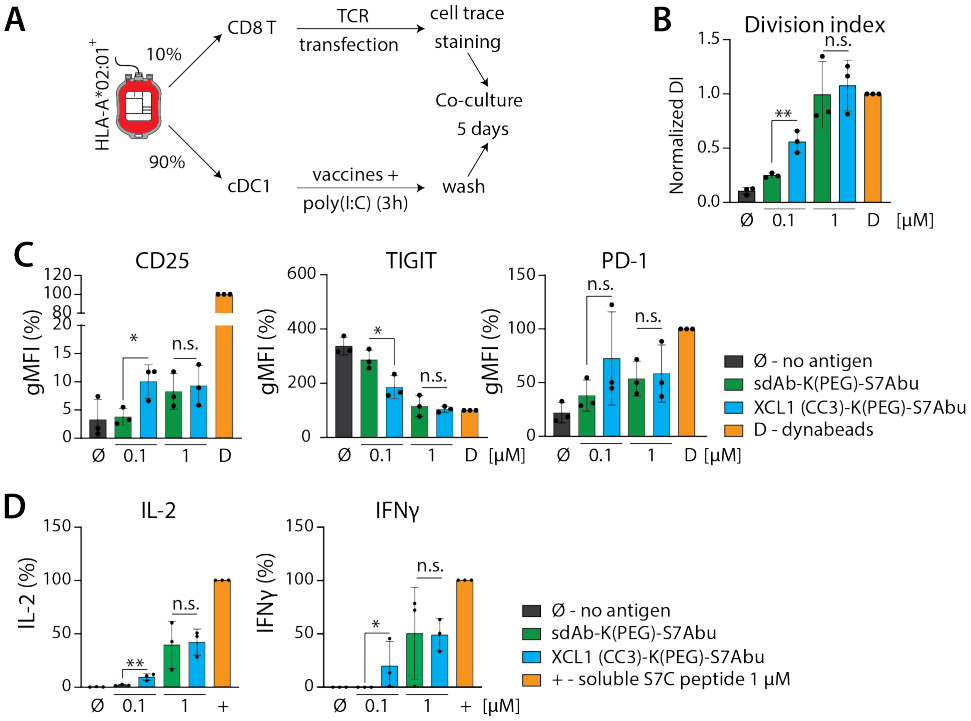

Figure 3 cDC1s treated with XCL1(CC3)-K(PEG)-S7Abu cross present S7Abu to CD8$^+$ T cells following XCR1-mediated uptake. (**A**) Experimental setup allowing for cdc1 isolation and CD8$^+$ T cell transfection with S7Abu-specific TCR. (**B, C, D**) increased activation of CD8$^+$ T cells through XCR1 targeting by cDC1s treated with XCL1(CC3)-K(PEG)-S7Abu (0.1 and 1 µM) compared with vehicle control, as measured by CD8$^+$ T cell division index (**B**), expression of activation markers (CD25, PD-1) and downregulation of TIGIT (**C**), and IL-2 and IFNγ secretion in the culture media (**D**). N=3 independent donors. One-way ANOVA with Tukey's post hoc correction for multiple testing, *p<0.05, **p<0.01. ANOVA, analysis of variance; ns, not significant.

shared frameshift neoantigens present in DNA-mismatch repair-deficient patients: TGFβRII (^{131}RLSSCVPV^{139}A, in short R7A),[28] and caspase 5 (^{67}FLIIWQNT^{75}M, in short F7M).[29] These epitopes display distinct properties from S7Abu: Y7A (hydrophobicity=22.80, GRAVY=0.08) is relatively hydrophilic, whereas R7A (hydrophobicity=19.88, GRAVY=0.98) is intermediate and F7M (hydrophobicity=38.19, GRAVY=0.99) is hydrophobic. After incorporating these epitopes in (GGG-K(N_3)-FR-X) backbones, we proceeded to subsequent peptide PEGylation (online supplemental figure S2G-I) and site-specific labeling of XCL1(CC3). The resulting XCL1(CC3)-antigen conjugates, XCL1(CC3)-K(PEG)-Y7A, XCL1(CC3)-K(PEG)-R7A and XCL1(CC3)-K(PEG)-F7M (figure 2E–G) were obtained using the same procedure as for S7Abu. These results illustrate the ability to generate XCL1(CC3)-antigen conjugates with a variety of tumor antigens and establish the versatility of our strategy.

XCL1(CC3)-K(PEG)-S7Abu elicits potent CD8$^+$ T cell responses following XCR1-mediated uptake by cDC1s

We analyzed the ability of primary human cDC1s exposed to XCL1(CC3)-K(PEG)-S7Abu to induce CD8$^+$ T cell proliferation and activation. To analyze the influence of XCR1 targeting, we also treated cDC1s with an unspecific vehicle (sdAb-K(PEG)-S7Abu) (figure 3A). CD8$^+$ T cells proliferated in response to presentation of their cognate antigen S7Abu on HLA-A*02:01 molecules in all conditions (figure 3B and online supplemental figure S3A). cDC1s treated with 0.1 µM XCL1(CC3)-K(PEG)-S7Abu induced an increased CD8$^+$ T cell proliferation compared with the control vehicle, as quantified by measuring CD8$^+$ T cell division index (figure 3B). In addition, CD8$^+$ T cells activated by cDC1s treated with 0.1 µM XCL1(CC3)-K(PEG)-S7Abu displayed an increased expression of IL2Rα (CD25), downregulated Interleukin-7 (IL-7) receptor (IL-7R) and T cell immunoreceptor with Ig and ITIM domains (TIGIT) (figure 3C and online supplemental figure S3B), and secreted increased levels of IL-2 and interferon γ (IFNγ) (figure 3D). Similarly, increased PD-1 and CD137 levels were detected, but this did not reach statistical significance (figure 3C and online supplemental figure S3B). cDC1s treated with higher doses (1 µM) of both XCR1-targeted and control constructs induced similar CD8$^+$ T cell proliferation, and activation (figure 3B–D).

To analyze the ability of XCL1-K(PEG)-S7Abu to target XCR1 on cDC1s in presence of other cells, we isolated cDC1s from CD3$^-$CD14$^-$CD19$^-$CD56$^-$ PBMCs of HLA-A*02:01$^+$ donors and used purified cDC2s or an excess of the unlabeled fraction (negative fraction, CD3$^-$CD14$^-$CD19$^-$CD56$^-$CD1c$^-$CD141$^-$) to spike the purified cDC1s (online supplemental figure S3C). We incubated the different DC mixtures with 0.1 µM XCL1-K(PEG)-S7Abu for 3 hours and analyzed their ability to activate CD8$^+$ T cells. cDC1s outperformed cDC2s to activate CD8$^+$ T cells. In addition, the presence of CD3$^-$CD14$^-$CD19$^-$CD56$^-$CD1c$^-$CD141$^-$ in a 10-fold excess did not affect cDC1-mediated CD8$^+$ T cell activation, suggesting that XCL1-K(PEG)-S7Abu might be able to selectively target XCR1 in

translational applications. Taken together, these results show that targeting of XCR1 increases tumor antigen uptake by cDC1s, resulting in an improved $CD8^+$ T cell activation.

DISCUSSION

In this study, we present a novel construct targeting human cDC1s. To the best of our knowledge, we show for the first time the potential of targeting XCR1 on peripheral blood human cDC1s for inducing antigen-specific $CD8^+$ T cell responses to a tumor antigen.

Functional analysis of XCL1(CC3) has shown dependency on the integrity of its *N*-, but not C-, terminus to bind XCR1.[16] XCL1 C-terminus can thus be used to introduce a site-specific modification site. Here, a functional chemokine, XCL1(CC3), stabilized in its XCR1 agonist fold,[20] and equipped with a C-terminal LPETGG sortag motif was designed and produced. C-terminal site-specific labeling of chemokines with small probes (<2 kDa) has been reported.[30–32] Therefore, conjugation of a fluorophore or a tumor antigen might be possible without disrupting its function. XCL1(CC3) selective binding to its target after conjugation to a small fluorophore was confirmed. SDS-PAGE analysis showed that XCL1(CC3) remained partially unreacted, indicating unfolded or misfolded XCL1(CC3), as detected by HPLC. Purity of the final product could be ensured by incubation with anti-FLAG beads, removing unreacted XCL1(CC3).

HLA-A*02:01 is a common haplotype, with a frequency averaging 45% in Europe depending on the ethnicity,[33 34] and therefore often exploited as model for (cancer) vaccines. The cancer testis antigen NY-ESO-1 contains an HLA-A*02:01 epitope (NY-ESO-1 (157–165), ^{157}SLLMWITQ^{165}C, in short S7C) known to elicit $CD8^+$ T cell responses in patients.[25] This peptide has low affinity for HLA-A*02:01 and has a cysteine anchor residue in P9 (^{165}Cys). This C-terminal cysteine causes problems in vaccine formulation due to oxidation. This prompted researchers to develop analogs of S7C[26 35] in efforts to generate more efficient cancer vaccines. Interestingly, variants of S7C displaying higher affinity for HLA-A*02:01 (^{157}SLLMWITQ^{165}V, ^{157}SLLMWITQ^{165}L)[35] did not show increased immunogenicity, and were not able to elicit cytotoxic T lymphocytes (CTLs) recognizing endogenously processed NY-ESO-1 (157-165). Substitution of the ^{165}Cys for ^{165}Abu, despite demonstrating weaker binding to HLA-A*02:01, showed increased immunogenicity on patient-derived $CD8^+$ T cells,[26] thus standing out as an ideal vaccine epitope.

While XCL1(CC3)-K(N_3)-S7Abu was formed in reaction, we were not able to stabilize it in solution, in spite of our efforts (cf. methods (Troubleshooting NY-ESO conjugation), for instance addition of glycerol,[36] or L-arginine·HCl solution[37]). S7C and its analogs are notoriously insoluble (solubility around 0.5 mM in DMSO, insoluble in ddH_2O and Tris-Cl buffer). The peptide was designed with an azido-lysine upstream of the epitope to have the flexibility for further functionalization via SPAAC; which was used to conjugate a 5 kDa PEG chain. PEGylation of proteins is a classical technique to increase hydrophilicity of poorly soluble compounds.[38 39] Excesses of triazole-PEG and K(PEG)-S7Abu were removed by cation exchange, and XCL1(CC3)-K(PEG)-S7Abu was purified with over 40% yield, with no detectable aggregation. Importantly, XCL1(CC3)-K(PEG)-S7Abu retained binding to XCR1, likely due to the site-specificity of the conjugation method. Moreover, primary human cDC1s exposed to XCL1(CC3)-K(PEG)-S7Abu were able to elicit antigen-specific $CD8^+$ T cell proliferation and activation, confirming that 5 kDa PEGylation did not prevent antigen processing and subsequent presentation on HLA-A*02:01 molecules.

TCR contact residues of immunogenic epitopes tend to be hydrophobic,[40] which is suggested to be a mechanism by which T cells discriminate immunogenic from tolerated epitopes.[41] This is consistent with observations that class I HLA-binding epitopes have a tendency to adopt native α-helical structures,[42 43] which are amphiphilic with a hydrophobic core. However, short polypeptides typically do not display α-helical structures in solution,[44] as it is not entropically favorable. Therefore, while it is not surprizing for short tumor antigens to be poorly soluble, it causes significant challenges in protein-based vaccine formulation. Here, a simple strategy was used, which enhanced peptide solubility and enabled conjugation to a targeting moiety, while not hindering binding, processing, and presentation by cDC1s. This strategy could be extended beyond the model epitope S7Abu, as demonstrated by generation of XCL1-antigen conjugates with epitopes of tumor antigens gp100 (Y7A), TGFβRII (R7A) and caspase 5 (F7M).

Importantly, XCL1(CC3)-K(PEG)-S7Abu retained chemotactic activity in vitro comparable to rhXCL1 and XCL1(CC3), demonstrating that site-specific modification and PEGylation of XCL1(CC3) did not impair chemokine functionality. In vivo, chemokines use GAG binding to establish gradients.[45 46] The underlying mechanism regulating GAG binding by chemokine oligomers[45] vs G protein-coupled receptor binding remains unknown. It is hypothesized that either GAG degradation by enzymes, and/or a change in concentration and equilibrium, regulates the local chemokine concentration. XCL1(CC3) in its α-β monomeric fold is reported to have low affinity for heparin, a member of the GAG family.[18 20] However, it remains very positively charged at physiological pH and could still interact with negatively charged GAGs, and thus generate chemokine gradients in vivo. To study whether this is the case, and whether it matters for therapeutic efficacy, a murine model or more elaborate in vitro model would be required. We hypothesize that co-administration of soluble FMS-like tyrosine kinase three ligand (FLT3L) would attract and induce differentiation of $XCR1^+$ DCs,[47] thus increasing the activity of the vaccine.

Data gathered from $CD8^+$ T cell activation assays revealed a dose-dependent activity of the constructs. XCL1(CC3)-K(PEG)-S7Abu was already active at low concentrations, and at 0.1 µM, displayed an increased activity compared with sdAb-K(PEG)-S7Abu. At 1 µM, $CD8^+$ T cell activation was enhanced, but both constructs induced a comparable response, as one would expect by exposing phagocytic cells to high amounts of soluble antigens.[48] These results revealed

a clear advantage of the XCL1(CC3) construct for targeted vaccination purposes. Notably, our data show that conjugate uptake is (partially) XCR1-mediated, and that targeting XCR1 on human cDC1s increases the efficacy of antigen presentation. These results are in line with previous research showing that targeting XCR1 in vivo increases the efficacy of antigen presentation.[13 49] Additionally, our data support a previous report of a hXCL1-glypican DNA-based vaccine,[15] able to chemo-attract lymph node-resident human cDC1s, which in turn activate antigen-specific T cells. DNA-based vaccines are advantageous due to their ease of manufacture; however, their low immunogenicity remains a key bottleneck.[50] Moreover, such a platform allows fusion of XCL1 to a hydrophilic protein, but conjugation to insoluble peptides, such as S7C, is not possible.

In conclusion, we produced a recombinant human XCR1 agonist (XCL1(CC3)) and developed a strategy to conjugate it to a poorly soluble epitope of a clinically relevant tumor antigen. We believe that this strategy is broadly applicable to other insoluble antigens and will solve a common formulation problem of protein-based fusion vaccines. The fusion construct retained XCR1 binding on primary human cDC1s and chemo-attractive properties. Moreover, cDC1s treated with XCL1(CC3)-K(PEG)-S7Abu induced potent $CD8^+$ T cell proliferation and activation. Our results show the potential of XCR1 as a promising target on peripheral blood human cDC1s to induce antigen-specific $CD8^+$ T cell immune responses.

Author affiliations
[1]Department of Tumor Immunology, Radboudumc Radboud Institute for Molecular Life Sciences, Nijmegen, The Netherlands
[2]Department of Tumor Immunology, Oncode Institute, Nijmegen, The Netherlands
[3]Institute for Chemical Immunology, Nijmegen, The Netherlands

Acknowledgements We thank Prof. Dr. Ton N.M. Schumacher (NKI, Amsterdam, NL) for permission to use the TCR sequence, and Prof. Dr. Uğur Şahin and Dr. Mustafa Diken (BioNTech, Mainz, DE) for providing mRNA encoding the TCR recognizing the NY-ESO-1 (157-165) epitope. We thank Dr. Marc Dalod for advice during project design.

Contributors CLG, GF-G and MV conceived the project and designed experiments with the help of IJMdV and CGF. CLG, AC, LdH and GF-G performed experiments. CLG and AC analyzed the data under supervision from GF-G and MV. IR-T, JC-E, KS, ZW, AMDB, JB and YD contributed experimentally. CLG and MV wrote the manuscript with assistance from all authors. MV is guarantor of this study. All authors reviewed the manuscript.

Funding This work was supported by ERC Starting grant CHEMCHECK (679921), a Gravity Program Institute for Chemical Immunology tenure track grant by NWO, the Oncode institute and EU grant PRECIOUS (686089). CGF is the recipient of the European Research Council (ERC) Advanced grant ARTimmune (834618).

Competing interests No, there are no competing interests.

Patient consent for publication Not applicable.

Ethics approval This study involves human participants and was approved by CMO Arnhem Nijmegen. Written informed consent was obtained for human sample collection, with approval from CMO Arnhem Nijmegen. Participants gave informed consent to participate in the study before taking part.

Provenance and peer review Not commissioned; externally peer reviewed.

Data availability statement Data are available in a public, open access repository. Data are available upon reasonable request.

ORCID iDs
Camille Le Gall http://orcid.org/0000-0002-5890-5115
Anna Cammarata http://orcid.org/0000-0001-9230-5132
Lukas de Haas http://orcid.org/0000-0003-1775-3570
Iván Ramos-Tomillero http://orcid.org/0000-0003-1928-4149
Jorge Cuenca-Escalona http://orcid.org/0000-0002-4915-1518
Kayleigh Schouren http://orcid.org/0000-0002-3546-3027
Zacharias Wijfjes http://orcid.org/0000-0001-5705-1624
Anouk M D Becker http://orcid.org/0000-0002-4758-9030
Johanna Bödder http://orcid.org/0000-0002-0183-1442
Yusuf Dölen http://orcid.org/0000-0001-8211-9811
I Jolanda M de Vries http://orcid.org/0000-0002-8653-4040
Carl G Figdor http://orcid.org/0000-0002-2366-9212
Georgina Flórez-Grau http://orcid.org/0000-0003-4431-985X
Martijn Verdoes http://orcid.org/0000-0001-8753-3528

REFERENCES

1 Sancho D, Joffre OP, Keller AM, *et al*. Identification of a dendritic cell receptor that couples sensing of necrosis to immunity. *Nature* 2009;458:899–903.
2 Zelenay S, Keller AM, Whitney PG, *et al*. The dendritic cell receptor DNGR-1 controls endocytic handling of necrotic cell antigens to favor cross-priming of CTLs in virus-infected mice. *J Clin Invest* 2012;122:1615–27.
3 Hildner K, Edelson BT, Purtha WE, *et al*. *Batf3* Deficiency Reveals a Critical Role for $CD8\alpha^+$Dendritic Cells in Cytotoxic T Cell Immunity. *Science* 2008;322:1097–100.
4 den Haan JM, Lehar SM, Bevan MJ. CD8(+) but not CD8(-) dendritic cells cross-prime cytotoxic T cells in vivo. *J Exp Med* 2000;192:1685–96.
5 Iyoda T, Shimoyama S, Liu K, *et al*. The CD8+ dendritic cell subset selectively endocytoses dying cells in culture and in vivo. *J Exp Med* 2002;195:1289–302.
6 Jongbloed SL, Kassianos AJ, McDonald KJ, *et al*. Human CD141+ (BDCA-3)+ dendritic cells (DCs) represent a unique myeloid DC subset that cross-presents necrotic cell antigens. *J Exp Med* 2010;207:1247–60.
7 Bachem A, Güttler S, Hartung E, *et al*. Superior antigen cross-presentation and XCR1 expression define human CD11c+CD141+ cells as homologues of mouse CD8+ dendritic cells. *J Exp Med* 2010;207:1273–81.
8 Dorner BG, Dorner MB, Zhou X, *et al*. Selective expression of the chemokine receptor XCR1 on cross-presenting dendritic cells determines cooperation with CD8+ T cells. *Immunity* 2009;31:823–33.
9 Lei Y, Ripen AM, Ishimaru N, *et al*. Aire-dependent production of XCL1 mediates medullary accumulation of thymic dendritic cells and contributes to regulatory T cell development. *J Exp Med* 2011;208:383–94.
10 Fox JC, Thomas MA, Dishman AF, *et al*. Structure-Function guided modeling of chemokine-GPCR specificity for the chemokine XCL1 and its receptor XCR1. *Sci Signal* 2019;12:eaat4128.
11 Marchese A, Paing MM, Temple BRS, *et al*. G protein-coupled receptor sorting to endosomes and lysosomes. *Annu Rev Pharmacol Toxicol* 2008;48:601–29.
12 Ohl L, Mohaupt M, Czeloth N, *et al*. Ccr7 governs skin dendritic cell migration under inflammatory and steady-state conditions. *Immunity* 2004;21:279–88.
13 Fossum E, Grødeland G, Terhorst D, *et al*. Vaccine molecules targeting XCR1 on cross-presenting DCs induce protective

CD8+ T-cell responses against influenza virus. *Eur J Immunol* 2015;45:624–35.
14 Botelho NK, Tschumi BO, Hubbell JA, *et al*. Combination of synthetic long peptides and XCL1 fusion proteins results in superior tumor control. *Front Immunol* 2019;10:1–11.
15 Chen K, Wu Z, Zhao H, *et al*. *XCL1/Glypican-3* Fusion Gene Immunization Generates Potent Antitumor Cellular Immunity and Enhances Anti-PD-1 Efficacy. *Cancer Immunol Res* 2020;8:81–93.
16 Kroczek AL, Hartung E, Gurka S, *et al*. Structure-Function Relationship of XCL1 Used for *in vivo* Targeting of Antigen Into XCR1$^+$ Dendritic Cells. *Front Immunol* 2018;9:2806.
17 Corgnac S, Botelho NK, Donda A, *et al*. Recombinant fusion proteins for targeting dendritic cell subsets in therapeutic cancer vaccine. *Methods Enzymol* 2020;632:521–43.
18 Tuinstra RL, Peterson FC, Kutlesa S, *et al*. Interconversion between two unrelated protein folds in the lymphotactin native state. *Proc Natl Acad Sci U S A* 2008;105:5057–62.
19 Fox JC, Nakayama T, Tyler RC, *et al*. Structural and agonist properties of XCL2, the other member of the C-chemokine subfamily. *Cytokine* 2015;71:302–11.
20 Tuinstra RL, Peterson FC, Elgin ES, *et al*. An engineered second disulfide bond restricts lymphotactin/XCL1 to a chemokine-like conformation with XCR1 agonist activity. *Biochemistry* 2007;46:2564–73.
21 Guimaraes CP, Witte MD, Theile CS, *et al*. Site-Specific C-terminal and internal loop labeling of proteins using sortase-mediated reactions. *Nat Protoc* 2013;8:1787–99.
22 van Rhee F, Szmania SM, Zhan F, *et al*. Ny-Eso-1 is highly expressed in poor-prognosis multiple myeloma and induces spontaneous humoral and cellular immune responses. *Blood* 2005;105:3939–44.
23 Rodolfo M, Luksch R, Stockert E, *et al*. Antigen-Specific immunity in neuroblastoma patients: antibody and T-cell recognition of NY-ESO-1 tumor antigen. *Cancer Res* 2003;63:6948–55.
24 Barrow C, Browning J, MacGregor D, *et al*. Tumor antigen expression in melanoma varies according to antigen and stage. *Clin Cancer Res* 2006;12:764–71.
25 Valmori D, Dutoit V, Liénard D, *et al*. Naturally occurring human lymphocyte antigen-A2 restricted CD8+ T-cell response to the cancer testis antigen NY-ESO-1 in melanoma patients. *Cancer Res* 2000;60:4499–506.
26 Webb AI, Dunstone MA, Chen W, *et al*. Functional and structural characteristics of NY-ESO-1-related HLA A2-restricted epitopes and the design of a novel immunogenic analogue. *J Biol Chem* 2004;279:23438–46.
27 Swee LK, Guimaraes CP, Sehrawat S, *et al*. Sortase-mediated modification of αDEC205 affords optimization of antigen presentation and immunization against a set of viral epitopes. *Proc Natl Acad Sci U S A* 2013;110:1428–33.
28 Saeterdal I, Gjertsen MK, Straten P, *et al*. A TGF betaRII frameshift-mutation-derived CTL epitope recognised by HLA-A2-restricted CD8+ T cells. *Cancer Immunol Immunother* 2001;50:469–76.
29 Schwitalle Y, Linnebacher M, Ripberger E, *et al*. Immunogenic peptides generated by frameshift mutations in DNA mismatch repair-deficient cancer cells. *Cancer Immun* 2004;4:14.
30 Popp MW, Antos JM, Grotenbreg GM, *et al*. Sortagging: a versatile method for protein labeling. *Nat Chem Biol* 2007;3:707–8.
31 Atterberry PN, Roark TJ, Severt SY, *et al*. Sustained delivery of chemokine CXCL12 from chemically modified silk hydrogels. *Biomacromolecules* 2015;16:1582–9.
32 Fang T, Li R, Li Z, *et al*. Remodeling of the tumor microenvironment by a Chemokine/Anti-PD-L1 nanobody fusion protein. *Mol Pharm* 2019;16:2838–44.
33 Gonzalez-Galarza FF, McCabe A, Santos EJMD, *et al*. Allele frequency net database (AFND) 2020 update: gold-standard data classification, open access genotype data and new query tools. *Nucleic Acids Res* 2020;48:D783–8.
34 Ryder LP, Andersen E, Svejgaard A. An HLA map of Europe. *Hum Hered* 1978;28:171–200.
35 Chen JL, Dunbar PR, Gileadi U, *et al*. Identification of NY-ESO-1 peptide analogues capable of improved stimulation of tumor-reactive CTL. *J Immunol* 2000;165:948–55.
36 Vagenende V, Yap MGS, Trout BL. Mechanisms of protein stabilization and prevention of protein aggregation by glycerol. *Biochemistry* 2009;48:11084–96.
37 Tischer A, Lilie H, Rudolph R, *et al*. L-Arginine hydrochloride increases the solubility of folded and unfolded recombinant plasminogen activator rPA. *Protein Sci* 2010;19:1783–95.
38 Goodson RJ, Katre NV. Site-Directed PEGylation of recombinant interleukin-2 at its glycosylation site. *Nat Biotechnol* 1990;8:343–6.
39 Veronese FM, Mero A. The impact of PEGylation on biological therapies. *BioDrugs* 2008;22:315–29.
40 Chowell D, Krishna S, Becker PD, *et al*. Tcr contact residue hydrophobicity is a hallmark of immunogenic CD8+ T cell epitopes. *Proc Natl Acad Sci U S A* 2015;112:E1754–62.
41 Huang L, Kuhls MC, Eisenlohr LC. Hydrophobicity as a driver of MHC class I antigen processing. *Embo J* 2011;30:1634–44.
42 Berkower I, Buckenmeyer GK, Berzofsky JA. Molecular mapping of a histocompatibility-restricted immunodominant T cell epitope with synthetic and natural peptides: implications for T cell antigenic structure. *J Immunol* 1986;136:2498–503.
43 Yusim K, Kesmir C, Gaschen B, *et al*. Clustering patterns of cytotoxic T-lymphocyte epitopes in human immunodeficiency virus type 1 (HIV-1) proteins reveal imprints of immune evasion on HIV-1 global variation. *J Virol* 2002;76:8757–68.
44 Forood B, Feliciano EJ, Nambiar KP. Stabilization of alpha-helical structures in short peptides via end capping. *Proc Natl Acad Sci U S A* 1993;90:838–42.
45 Proudfoot AEI, Handel TM, Johnson Z, *et al*. Glycosaminoglycan binding and oligomerization are essential for the in vivo activity of certain chemokines. *Proc Natl Acad Sci U S A* 2003;100:1885–90.
46 Handel TM, Johnson Z, Crown SE, *et al*. Regulation of protein function by glycosaminoglycans--as exemplified by chemokines. *Annu Rev Biochem* 2005;74:385–410.
47 Hammerich L, Marron TU, Upadhyay R, *et al*. Systemic clinical tumor regressions and potentiation of PD1 blockade with in situ vaccination. *Nat Med* 2019;25:814–24.
48 Flacher V, Tripp CH, Stoitzner P, *et al*. Epidermal Langerhans cells rapidly capture and present antigens from C-type lectin-targeting antibodies deposited in the dermis. *J Invest Dermatol* 2010;130:755–62.
49 Lysén A, Braathen R, Gudjonsson A, *et al*. Dendritic cell targeted Ccl3- and Xcl1-fusion DNA vaccines differ in induced immune responses and optimal delivery site. *Sci Rep* 2019;9:1–11.
50 MacGregor RR, Boyer JD, Ugen KE, *et al*. First human trial of a DNA-based vaccine for treatment of human immunodeficiency virus type 1 infection: safety and host response. *J Infect Dis* 1998;178:92–100.
51 Reddy K RC, Lilie H, Rudolph R, *et al*. L-Arginine increases the solubility of unfolded species of hen egg white lysozyme. *Protein Sci* 2005;14:929–35.
52 Lyon RP, Bovee TD, Doronina SO, *et al*. Reducing hydrophobicity of homogeneous antibody-drug conjugates improves pharmacokinetics and therapeutic index. *Nat Biotechnol* 2015;33:733–5.